Investigation of ACE2 N-terminal fragments binding to SARS-CoV-2 Spike RBD

Authors: G. Zhang[1], S. Pomplun[1], A. R. Loftis[1], X. Tan[1], A. Loas[1], and B. L. Pentelute[1,2*]

Affiliations:

[1] Massachusetts Institute of Technology, Department of Chemistry, 77 Massachusetts Avenue, Cambridge, MA 02139, USA.

[2] Extramural Member, Koch Institute of Integrative Cancer Research MIT; Associate Member, Broad Institute of MIT and Harvard; Member, Center for Environmental Health Sciences MIT; Cambridge, MA 02139, USA.

*Correspondence to: blp@mit.edu

Abstract

Coronavirus disease 19 (COVID-19) is an emerging global health crisis. With over 7 million confirmed cases to date, this pandemic continues to expand, spurring research to discover vaccines and therapies. SARS-CoV-2 is the novel coronavirus responsible for this disease. It initiates entry into human cells by binding to angiotensin-converting enzyme 2 (ACE2) via the receptor binding domain (RBD) of its spike protein (S). Disrupting the SARS-CoV-2-RBD binding to ACE2 with designer drugs has the potential to inhibit the virus from entering human cells, presenting a new modality for therapeutic intervention. Peptide-based binders are an attractive solution to inhibit the RBD-ACE2 interaction by adequately covering the extended protein contact interface. Using molecular dynamics simulations based on the recently solved cryo-EM structure of ACE2 in complex with SARS-CoV-2-RBD, we observed that the ACE2 peptidase domain (PD) α1 helix is important for binding SARS-CoV-2-RBD. Using automated fast-flow peptide synthesis, we chemically synthesized a 23-mer peptide fragment of the ACE2 PD α1 helix (SBP1) composed entirely of proteinogenic amino acids. Chemical synthesis of SBP1 was complete in 1.5 hours, and after work up and isolation >20 milligrams of pure material was obtained. Bio-layer interferometry (BLI) revealed that SBP1 associates with micromolar affinity to insect-derived SARS-CoV-2-RBD protein obtained from Sino Biological. Association of SBP1 was not observed to an appreciable extent to HEK cell-expressed SARS-CoV-2-RBD proteins and insect-derived variants acquired from other vendors. Moreover, competitive BLI assays showed SBP1 does not outcompete ACE2 binding to Sino Biological insect-derived SARS-CoV-2-RBD. Further investigations are ongoing to gain insight into the molecular and structural determinants of the variable binding behavior to different SARS-CoV-2-RBD protein variants.

Key words：SARS-CoV-2, peptide binder, protein-protein interaction inhibitor, coronavirus, COVID-19, rapid response, MD simulation, automated flow peptide synthesis

53 **1. Introduction**

54 A novel coronavirus (SARS-CoV-2) from Wuhan, China, has caused over 7 million
55 confirmed cases and over 400,000 deaths globally, according to the COVID-19 situation report
56 from WHO on June 10, 2020 (https://www.who.int/emergencies/diseases/novel-coronavirus-
57 2019/situation-reports/), and the number is continually growing. Similar to the SARS-CoV
58 outbreak in 2002, SARS-CoV-2 causes severe respiratory problems. Coughing, fever, difficulties
59 in breathing and/or shortage of breath are the common symptoms. Aged patients with pre-existing
60 medical conditions are at most risk with a mortality rate ~1.5% or even higher in some regions.
61 Moreover, human-to-human transmission can occur rapidly by close contact. To slow this
62 pandemic and treat infected patients, rapid development of specific antiviral drugs is of the highest
63 urgency.

64 The closely-related SARS-CoV coronavirus invades host cells by binding the angiotensin-
65 converting enzyme 2 (ACE2) receptor on human cell surface through its viral spike protein (S) [1-
66 4]. It was recently established that SARS-CoV-2 uses the same receptor for host cell entry and
67 binds ACE2 with an affinity comparable with the corresponding spike protein of SARS-CoV [5, 6].
68 Recent cryo-electron microscopy (cryo-EM) structural studies of the SARS-CoV-2 spike protein
69 receptor binding domain (RBD) in complex with full-length human ACE2 receptor revealed key
70 amino acid residues at the contact interface between the two proteins and estimated the binding
71 affinity at ~15 nM [7, 8]. These studies provide valuable information that can be leveraged for the
72 development of disruptors specific for the SARS-CoV-2/ACE2 protein-protein interaction (PPI).
73 Small-molecule inhibitors are often less effective at disrupting extended protein binding interfaces
74 [9]. Peptides, on the other hand, offer a synthetically accessible solution to disrupt PPIs by binding
75 at interface regions containing multiple contact “hot spots” [10].

76 We hypothesized that disruption of the viral SARS-CoV-2-RBD/host ACE2 interaction with
77 peptide-based binders would prevent virus entry into human cells, offering a novel opportunity for

78 therapeutic intervention. To investigate this hypothesis, we launched a campaign to design and
79 discover minimum-length peptide binders to SARS-CoV-2-RBD. Notably, coronavirus spike
80 proteins have been previously targeted with peptide-based fragments, such as an extended ACE2
81 helical mimic developed against SARS-CoV-RBD [11], pan-CoV inhibitors of the fusion of the
82 spike S2 subunit with the cell membrane [12, 13], and an 85-mer N-terminal truncate of the ACE2
83 protein that binds SARS-CoV-2-RBD with nanomolar affinity [14]. Complementing these
84 approaches, our efforts aimed to determine the minimum length required for an ACE2 N-terminal
85 peptide fragment that maintains specific association with SARS-CoV-2-RBD.

86 Analyzing the cryo-EM structure of the SARS-CoV-2-RBD/ACE2 complex, we found that
87 the binding interface spans a large elongated surface area, as is common for PPIs. We leveraged
88 molecular dynamics simulations and automated fast-flow peptide synthesis [15] to prepare a 23-
89 mer peptide binder (SBP1) to SARS-CoV-2-RBD, the sequence of which was derived from the
90 ACE2 α1 helix. Using bio-layer interferometry (BLI), we determined that N-terminal biotinylated
91 SBP1 binds Sino Biological insect-derived SARS-CoV-2-RBD with micromolar affinity
92 (dissociation constant, K_D = 1.3 μM). We also found, however, that N-terminal biotinylated SBP1
93 does not associate with HEK-expressed SARS-CoV-2-RBD or insect-derived variants purchased
94 from other commercial sources. Although biotinylated SBP1 binds Sino Biological insect-derived
95 SARS-CoV-2-RBD when immobilized on BLI streptavidin tips, no specific disruption of the SARS-
96 CoV-2-RBD/ACE2 interaction was observed in solution in a BLI competition assay. Further
97 investigation is currently ongoing to understand the different association behaviors of this ACE2-
98 derived peptide to SARS-CoV-2-RBD protein variants.

99 **2. Results**

100 **Molecular dynamic simulations guide peptide binder design**

101 Using the Amber force field[16] a helical peptide sequence (spike-binding peptide 1, SBP1)
102 derived from the α1 helix of ACE2 peptidase domain (ACE2-PD) in complex with SARS-CoV-2-

103 RBD was simulated under TIP3P explicit water conditions. Analyzing the simulation trajectory
104 after 200 ns, we found that SBP1 remains on the spike RBD protein surface in a stable
105 conformation (Fig. 2B) with overall residue fluctuations smaller than 0.8 nm compared with their
106 starting coordinates (Fig. 2A). Per-residue analysis along the 200 ns trajectory showed that the
107 middle residues of SBP1, a 12-mer sequence we termed SBP2, have significantly reduced
108 fluctuations (Fig. 2C, 2D), indicating key interactions. The results of this MD simulation suggest
109 that SBP1 and SBP2 peptides derived from the ACE-PD α1 helix may alone potentially bind the
110 SARS-CoV-2 spike RBD protein with sufficient affinity to disrupt the associated PPI.

111 **Automated fast-flow peptide synthesis yields >95% pure compound**

112 The two N-terminal biotinylated peptides, SBP1 and SBP2, derived from the α1 helix were
113 prepared by automated fast-flow peptide synthesis[15, 17] with a total synthesis time of 1.5 h over
114 35 coupling cycles. After cleavage from resin, global deprotection, and subsequent C18 solid-
115 phase extraction, the purity of the crude peptides was estimated to be >95% for both biotinylated
116 SBP1 and SBP2 based on LC-MS TIC chromatograms (Supplemental Fig. 1). We assessed this
117 purity as acceptable for direct downstream biological characterization.

118 **SBP1 peptide binds Sino Biological insect-derived SARS-CoV-2-RBD with micromolar**
119 **affinity, but does not associate with other commercial sources of SARS-CoV-2-RBD**

120 Bio-layer interferometry (BLI) was used to measure the binding affinity of the synthesized
121 peptide SBP1 to glycosylated Sino Biological insect-derived SARS-CoV-2-RBD, Sino Biological
122 HEK-expressed SARS-CoV-2-RBD, GenScript insect-derived SARS-CoV-2-RBD and
123 AcroBiosystems HEK-expressed SARS-CoV-2-RBD. In all of these assays, biotinylated SBP1
124 was immobilized onto streptavidin (SA) biosensors. After fitting the association and dissociation
125 curves from serial dilutions of the protein, the dissociation constant (K_D) of SBP1 to glycosylated
126 Sino Biological insect-derived SARS-CoV-2-RBD was determined to be ~1300 nM using the

127 global fitting algorithm and 1:1 binding model (Fig. 2E). However, SBP1 did not associate with the
128 other three SARS-CoV-2-RBD proteins studied (Fig. 2E). Surprisingly, a scrambled sequence of
129 SBP1 exhibited binding to the Sino Biological insect-derived SARS-CoV-2-RBD with comparable
130 association response to SBP1 at 500 nM concentration (Fig. 2E). SBP1 had no observable
131 binding to a negative control human protein menin (Fig. 2F). Likewise, no association was
132 observed between the biotinylated 12-mer SBP2 and Sino Biological insect-derived SARS-CoV-
133 2-RBD (Fig. 2F).

134 **SBP1 does not compete with biotinylated ACE2 binding to Sino Biological insect-derived**
135 **SARS-CoV-2-RBD**

136 Using a competition-format BLI assay, we confirmed that soluble human ACE2 protein
137 could compete with immobilized biotinylated ACE2 (AcroBiosystems) for binding Sino Biological
138 insect-derived SARS-CoV-2-RBD, and that a 5-fold excess of soluble ACE2 (relative to
139 immobilized biotinylated ACE2) abolished nearly all of the initial ACE2/RBD binding interaction
140 (Fig. 3B, 3D). However, competition was not observed when using non-biotinylated SBP1 pre-
141 mixed in solution with Sino Biological insect-derived SARS-CoV-2-RBD, even with a 1000-fold
142 excess of the peptide (Fig. 3C, 3E). These data suggest that SBP1 potentially binds SARS-CoV-
143 2-RBD at a different site than ACE2, binds SARS-CoV-2-RBD too weakly, or for other unknown
144 reasons cannot disrupt the native ACE2/RBD interaction.

145 **3. Discussion**

146 Recently published cryo-EM structures of the RBD of SARS-CoV-2 in complex with human
147 ACE2 have identified this PPI as a key step for the entry of SARS-CoV-2 into human cells [7, 8].
148 Blocking this binding interface represents a highly promising therapeutic strategy, as it could
149 potentially hinder cellular uptake of SARS-CoV-2 and intracellular replication.

150 Drugging PPIs is a longstanding challenge in traditional drug discovery and peptide-based
151 approaches might help to solve this problem. Small molecule compounds are unlikely to bind
152 large protein surfaces that do not have distinct binding pockets. Peptides, on the other hand,
153 display a larger surface area and chemical functionalities that can mimic and disrupt the native
154 PPI, as is the case for the clinically approved HIV peptide drug Fuzeon [18, 19].

155 The identification of a suitable starting point for drug discovery campaigns can be time-
156 intensive. During a pandemic such as this one, therapeutic interventions are urgently needed.
157 Peptide-based strategies were developed to target both the spike protein RBD and S2 subunit of
158 the first SARS-CoV virus [11,12]. Translating these approaches to SARS-CoV-2, inhibitors of the
159 spike protein fusion with the cell membrane and engineered mini-proteins that bind SARS-CoV-2
160 RBD were developed [13,14]. We aimed to determine the minimum length required of the ACE2
161 N-terminal peptide fragment in order to maintain binding affinity to SARS-CoV-2-RBD and thus
162 potentially deliver a synthetically accessible therapeutic candidate. To rapidly identify potential
163 short peptide binders to the SARS-CoV-2 spike protein, we used molecular dynamics (MD)
164 simulation on peptides extracted from the human ACE2 sequence. The starting point of the
165 binding simulations was the cryo-EM model of the SARS-CoV-2 spike protein and several
166 peptides derived from the SARS-CoV-2-spike binding domain of human ACE2 protein. Our MD
167 simulation (200 ns trajectory) indicated that the SBP1 peptide, corresponding to the N-terminal
168 ACE2 α1 helix, stably bound to SARS-CoV-2-RBD. The overall peptide fluctuations were smaller
169 than 0.8 nm from the starting coordinates (Fig. 2A). These results indicated the potential of
170 identifying a short SARS-CoV-2-RBD-binding peptide derived from the human ACE2 α1 helix.

171 A 23-mer peptide sequence (SBP1) was synthesized by automated flow peptide synthesis
172 [15]. The 23 residues selected from the ACE2 α1 helix sequence
173 (IEEQAKTFLDKFNHEAEDLFYQS) showed low fluctuations along the MD simulation trajectory
174 and several important interactions with the spike protein were observed consistently with multiple

175 lines of published data [8, 20]. We used this peptide (SBP1) as an experimental starting point for
176 the development of a SARS-CoV-2 spike protein binder. Our rapid automated flow peptide
177 synthesizer enabled the synthesis of tens of milligrams of SBP1 peptide within 1.5 h. The crude
178 purity was determined to be >95% and therefore sufficient for binding validation by BLI.

179 The interaction between N-terminal biotinylated SBP1 and the RBD of glycosylated SARS-
180 CoV-2 spike protein was investigated in detail. We performed serial dilutions of the soluble protein
181 to reliably determine the binding affinity of SBP1 to Sino Biological insect-derived SARS-CoV-2-
182 RBD. Using a global fitting algorithm, we found that N-terminal biotinylated SBP1 binds Sino
183 Biological insect-derived SARS-CoV-2-RBD with micromolar affinity (K_D = 1.3 μM), a value almost
184 100-times higher than the estimated binding affinity of the native ACE2 receptor (K_D ~ 15 nM [7])
185 (Fig. 2E). The decreased binding affinity relative to ACE2 may partially explain why SBP1 was
186 unable to significantly disrupt ACE2 binding to Sino Biological insect-derived SARS-CoV-2-RBD
187 even at 1000-fold excess in a BLI competition assay (Fig. 3C,E). In addition, the comparable
188 affinity observed for a scrambled sequence of SBP1 (Fig. 2E) suggests the possibility of a
189 promiscuous peptide binding site on the surface of glycosylated Sino Biological insect-derived
190 SARS-CoV-2-RBD at a different location than the one involved in ACE2 receptor binding.

191 An important outcome of our preliminary BLI binding studies relates to the significantly
192 different SBP1 association behavior observed toward the various SARS-CoV-2-RBD commercial
193 sources investigated. Among the four variants (two insect-derived and two HEK-expressed), Sino
194 Biological insect-derived SARS-CoV-2-RBD was the only one displaying observable association
195 with SBP1 in the BLI Octet assay. This behavior may be partially ascribed to variability in the site-
196 specific patterns and surface density of SARS-CoV-2-RBD post-translational modifications
197 (PTMs), in particular glycosylation [21], imparted by the different biological expression sources.
198 Distinct PTM patterns are evident in the different mass distribution envelopes obtained by
199 deconvolution of the Sino Biological insect-derived and HEK-expressed SARS-CoV-2-RBD

200 protein total ion current bands, respectively, analyzed by LC-MS (Supplemental Fig. 2). Access
201 to non-glycosylated SARS-CoV-2-RBD either by bacterial recombinant expression or total
202 chemical synthesis in flow [15] may provide additional insight into the role of glycans in modulating
203 peptide interactions with the SARS-CoV-2-RBD/ACE2 interface. Investigations along these lines
204 are in progress to gain additional understanding of these molecular processes.

205 In conclusion, a biotinylated peptide sequence derived from human ACE2 was found to
206 bind Sino Biological insect-derived SARS-CoV-2 spike protein RBD with micromolar affinity, but
207 did not associate with SARS-CoV-2-RBD variants obtained from other commercial sources. In
208 spite of this association, competitive BLI data indicates that SBP1, even at 1000-fold excess, did
209 not compete with ACE2 for binding to SARS-CoV-2-RBD. Our preliminary studies highlight the
210 unexpected challenges researchers may encounter while developing peptide-based approaches
211 to disrupt the specific interactions of SARS-CoV-2 with its mammalian cell membrane receptors.
212 At the same time, the BLI experiments draw attention to the wide variability in the behavior of the
213 SARS-CoV-2 spike protein variants in solution, likely a consequence of the biological expression
214 source, manufacturing and/or formulation protocols. The development of peptide-based
215 disruptors of SARS-CoV-2 cell entry effective in a clinical setting relies on a broader evaluation
216 and understanding of its spike protein isoforms.

217 4. Experimental Materials and Methods

218 GPU-accelerated molecular dynamic simulation

219 The cryo-EM structure of ternary complex of SARS-CoV-2-RBD with ACE2-B^{0}AT1 (PDB: 6M17)
220 was chosen as the initial structure, which was explicitly solvated in an 87 Å^3 box, to perform a 200
221 ns molecular dynamical (MD) simulation using NAMD on MIT's supercomputing clusters (GPU
222 node). The Amber force field was used to model the protein and peptide. The MD simulation
223 system was equilibrated at 300 K for 2 ns. Periodic boundary conditions were used and long-

224 range electrostatic interactions were calculated with particle mesh Ewald method, with non-
225 bonded cutoff set to 12.0 Å. SHAKE algorithm was used to constrain bonds involving hydrogen
226 atoms. Time step is 2 fs and the trajectories were recorded every 10 ps. After simulation
227 production runs, trajectory files were loaded into the VMD software for further analysis.

228 **Automated fast-flow peptide synthesis**

229 SBP1 and SBP2 sequences were synthesized at 90 °C on Rink Amide-ChemMatrix resin with
230 HATU activation using a fully automatic flow-based peptide synthesizer. Amide bond formation
231 was performed in 8 seconds, and Fmoc groups were removed in 8 seconds with 40% (v/v)
232 piperidine in DMF. The overall synthesis cycle was completed in ~120 seconds per amino acid
233 incorporated. After completion of fast-flow synthesis, the resins were washed with DMF (3 x) and
234 then incubated with HATU-activated biotin-PEG_4-propionic acid (CAS# 721431-18-1) at room
235 temperature for 1.0 h for biotinylation on the peptide N-terminus.

236 **Peptide cleavage and deprotection**

237 After peptide synthesis, the peptidyl resin was rinsed with dichloromethane briefly and then dried
238 in a vacuum chamber overnight. Next day, approximately 5 mL of cleavage solution (94%
239 trifluoroacetic acid (TFA), 1% TIPS, 2.5% EDT, 2.5% water) was added into the syringe containing
240 the resin. The syringe was kept at room temperature for 2 h before injecting the cleavage solution
241 into a 50 mL conical tube. Dry-ice cold diethyl ether (~50 mL) was added to the cleavage mixture
242 and the precipitate was collected by centrifugation and triturated twice with cold diethyl ether (50
243 mL). The supernatant was discarded. Residual ether was allowed to evaporate and the peptide
244 was dissolved in water with 0.1% TFA for solid-phase extraction.

245 **Solid-phase extraction (SPE)**

246 After peptide cleavage, peptide precipitates were dissolved in water with 0.1% TFA. Agilent Mega
247 BE C18 column (Part No: 12256130) was conditioned with 5 mL of 100% acetonitrile with 0.1%

248 TFA, and then equilibrated with 15 mL of water with 0.1% TFA. Peptides were loaded onto the
249 column for binding, followed by washing with 15 mL of water with 0.1% TFA, and finally, eluted
250 with 5 mL of 30/70 water/acetonitrile (v/v) with 0.1% TFA.

251 **Liquid chromatography-mass spectrometry (LC-MS)**

252 Peptides were dissolved in water with 0.1% TFA followed by LC-MS analysis on an Agilent 6550
253 iFunnel ESI-Q-ToF instrument using an Agilent Jupiter C4 reverse-phase column (2.1 mm × 150
254 mm, 5 μm particle size). Mobile phases were 0.1% formic acid in water (solvent A) and 0.1%
255 formic acid in acetonitrile (solvent B). Linear gradients of 1 to 61% solvent B over 15 minutes (flow
256 rate: 0.5 mL/min) were used to acquire LC-MS chromatograms.

257 **Kinetic binding assay using bio-layer interferometry (BLI)**

258 A ForteBio Octet® RED96 Bio-Layer Interferometry system (Octet RED96, ForteBio, CA) was
259 used to characterize the in vitro peptide-protein binding affinity at 30 °C and 1000 rpm. Briefly,
260 streptavidin (SA) tips were dipped in 200 μL of biotinylated peptide solution (2.5 μM in 1x kinetic
261 buffer: 1x PBS with 0.1% BSA and 0.05% tween) for the loading step. The tips loaded with peptide
262 were then sampled with four different sourced SARS-CoV-2-RBD proteins (Sino Biological insect-
263 derived RBD, CAT: 40592-V08B; Sino Biological HEK-expressed RBD, CAT: 40592-V08H;
264 AcroBiosystems HEK-expressed RBD, CAT: SPD-C52H3; GenScript insect-derived RBD, CAT:
265 Z03479) or menin protein at various concentrations in 1x kinetic buffer to obtain the association
266 curve. Peptide only was used as reference for background subtraction. After association, the tips
267 were dipped back into 1x kinetic buffer to obtain the dissociation curve. The association and
268 dissociation curves were fitted with ForteBio Biosystems using four experimental conditions (n =
269 6, global fitting algorithm, binding model 1:1) to obtain the dissociation constants K_D.

270

271

272 **In-solution BLI competition assay**

273 A BLI competition binding assay was set up as previously described.[22] First, a calibration curve
274 was constructed using biotinylated ACE2 dipping into a serially-diluted Sino Biological insect-
275 derived SARS-CoV-2-RBD. In brief, streptavidin sensors were soaked in kinetic buffer (PBS
276 supplemented with 0.02% Tween-20, and 0.1% BSA) for 10 min at 30 °C, and loaded with
277 biotinylated ACE2 for 4 min. Then, serial dilutions of SARS-CoV-2-RBD in Kinetic buffer were
278 analyzed for binding, typically at 30 °C and 1,000 rpm. Second, with the binding information from
279 the calibration curve, a concentration of SARS-CoV-2-RBD protein at 100 nM was chosen to
280 premix with various concentration of SBP1 to study the competition effects. Briefly, different
281 concentration of SBP1 was incubated with 100 nM Sino Biological insect-derived SARS-CoV-2-
282 RBD protein at room temperature for 15 min. Meanwhile, streptavidin sensors were soaked into
283 kinetic buffer for 10 min at 30 °C. ACE2 was immobilized on the streptavidin sensor surface and
284 the association and dissociation curves of SARS-CoV-2-RBD in the preincubated samples were
285 then analyzed at 30 °C and 1,000 rpm.

286 **Acknowledgements**

287 The authors thank the MIT Supercomputing Center for providing the computational
288 resources to run MD simulations. This research was supported by a COVID-19 Fast Grant award
289 sponsored by Emergent Ventures at the Mercatus Center, George Mason University, and by MIT
290 seed funds. S.P. is supported by a postdoctoral fellowship from Deutsche
291 Forschungsgemeinschaft (DFG, award PO 2413/1-1). MIT has filed a provisional patent
292 application related to this work.

293 **Competing interests**

294 B.L.P. is a founder of Resolute Bio and Amide Technologies.

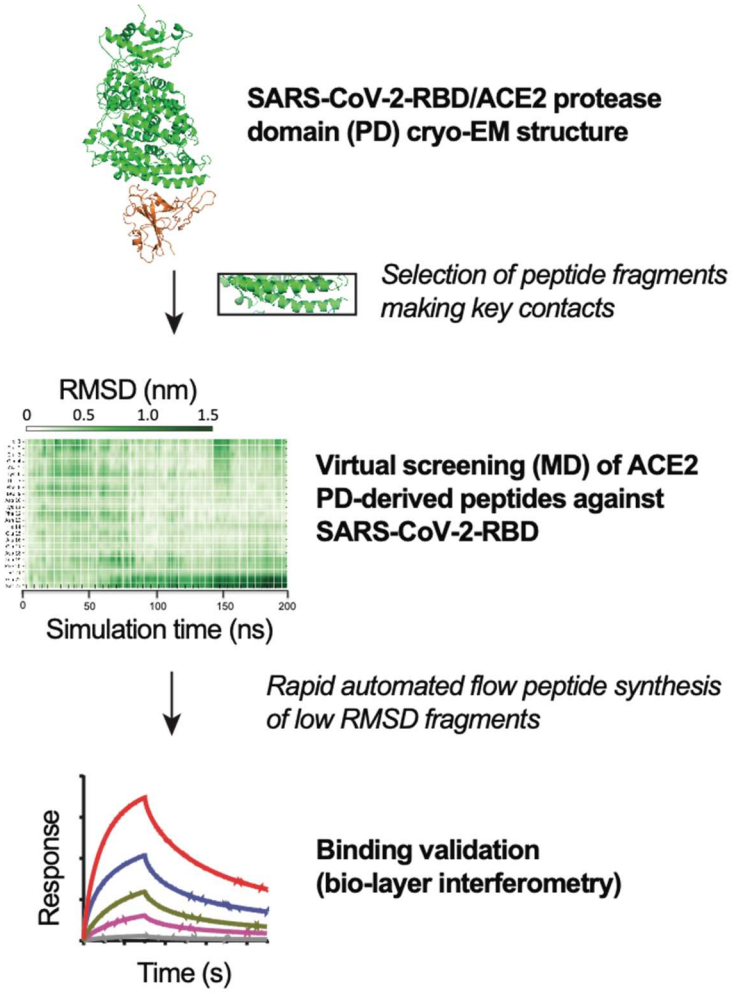

295

296 **Figure 1. MD-guided target selection for rapid flow synthesis of a SARS-CoV-2-RBD-**
297 **binding peptide.** Fragments of ACE2-PD domain are docked against SARS-CoV-2 receptor-
298 binding domain (PDB: 6M17). Low RMSD peptides are rapidly synthesized by fully automated
299 flow peptide synthesis, and binding to glycosylated SARS-CoV-2-RBD is determined by BLI.

300

301

302

303

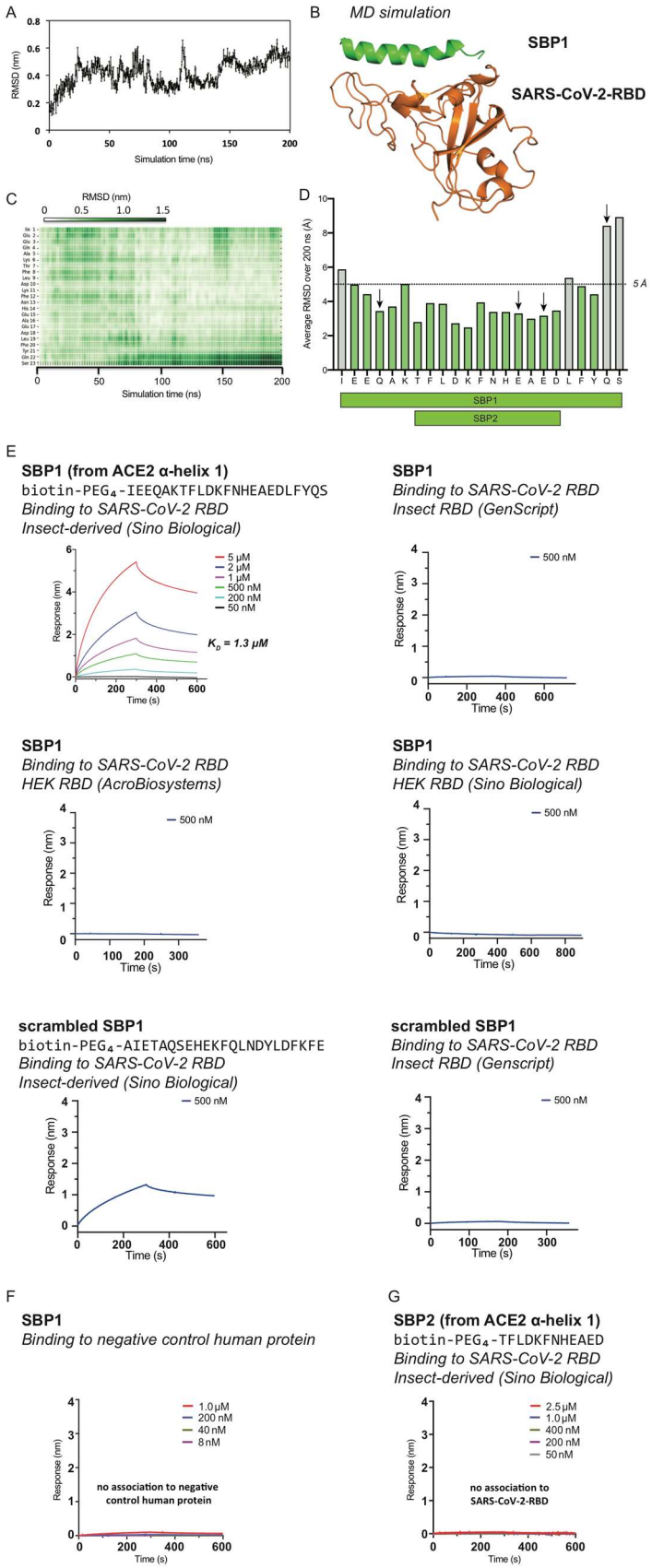
A
RMSD (nm)
Simulation time (ns)
B
MD simulation
SBP1
SARS-CoV-2-RBD
C
RMSD (nm)
Simulation time (ns)
D
Average RMSD over 200 ns (Å)
5 Å
I E E Q A K T F L D K F N H E A E D L F Y Q S
SBP1
SBP2
E
SBP1 (from ACE2 α-helix 1)
biotin-PEG4-IEEQAKTFLDKFNHEAEDLFYQS
Binding to SARS-CoV-2 RBD
Insect-derived (Sino Biological)
5 μM
2 μM
1 μM
500 nM
200 nM
50 nM
K_D = 1.3 μM
Response (nm)
Time (s)
SBP1
Binding to SARS-CoV-2 RBD
Insect RBD (GenScript)
500 nM
SBP1
Binding to SARS-CoV-2 RBD
HEK RBD (AcroBiosystems)
SBP1
Binding to SARS-CoV-2 RBD
HEK RBD (Sino Biological)
scrambled SBP1
biotin-PEG4-AIETAQSEHEKFQLNDYLDFKFE
Binding to SARS-CoV-2 RBD
Insect-derived (Sino Biological)
scrambled SBP1
Binding to SARS-CoV-2 RBD
Insect RBD (Genscript)
F
SBP1
Binding to negative control human protein
1.0 μM
200 nM
40 nM
8 nM
no association to negative control human protein
G
SBP2 (from ACE2 α-helix 1)
biotin-PEG4-TFLDKFNHEAED
Binding to SARS-CoV-2 RBD
Insect-derived (Sino Biological)
2.5 μM
1.0 μM
400 nM
200 nM
50 nM
no association to SARS-CoV-2-RBD

304

305 **Figure 2. Human ACE2-PD domain α-helix 1-derived SBP1 binds only Sino Biological**
306 **insect-derived SARS-CoV-2-RBD.** (A) RMSD for SBP1 docked to SARS-CoV-2-RBD during 200
307 ns MD simulation. (B) Binding interface between SARS-CoV-2-RBD and SBP1 after 200 ns
308 simulation. Individual RMSD (C) and average RMSD (D) values for SBP1 residues over the
309 course of the 200 ns simulation. Arrows indicate residues contributing key hydrogen bonding
310 interactions (determined using UCSF Chimera, Version 1.12). Individual residues with RMSD
311 below 5 Å arbitrarily colored green. (E) Binding affinity of SBP1 and a scrambled SBP1 sequence
312 to various sources of glycosylated SARS-CoV-2-RBD proteins determined by bio-layer
313 interferometry (BLI). (F) BLI association response of SBP1 to negative control human protein
314 menin and (G) BLI association response of 12-mer SBP2 peptide to Sino Biological insect-derived
315 SARS-CoV-2-RBD.

316

317

318

319

320

321

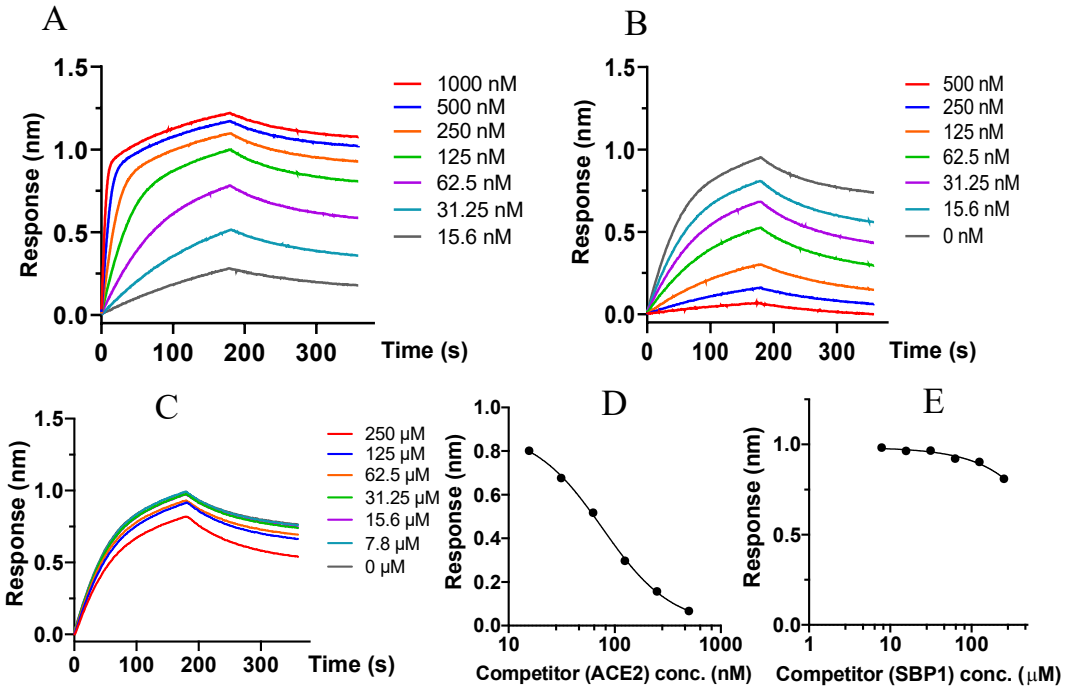

Figure 3. SBP1 does not compete with ACE2 binding to Sino Biological insect-derived SARS-CoV-2-RBD. (A) Association responses of biotinylated ACE2 to Sino Biological insect-derived SARS-CoV-2-RBD at different concentrations. The kinetic dissociation constant determined under these conditions was $K_{D,\ ACE2}$ = 15 nM. (B and D) Association responses of biotinylated ACE2 with Sino Biological insect-derived SARS-CoV-2-RBD (kept constant at 100 nM) after mixing with soluble human ACE2 at different concentrations. (B) shows the BLI traces and (D) shows re-plots of the endpoint association response (nm) as a function of ACE2 concentration. (C and E) Association responses of biotinylated ACE2 with Sino Biological insect-derived SARS-CoV-2-RBD (kept constant at 100 nM) after mixing with SBP1 at different concentrations. (C) shows the BLI traces and (E) shows re-plots of the endpoint association response (nm) as a function of SBP1 concentration.

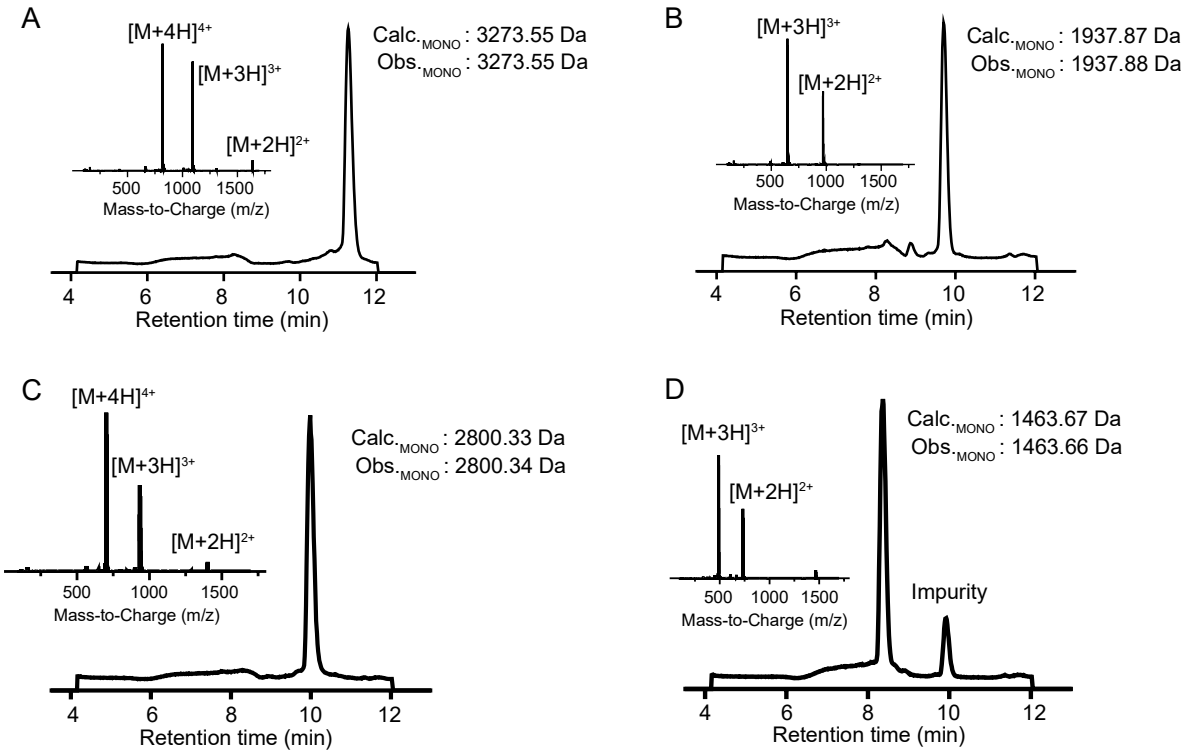

Supplemental Figure 1. ACE2-derived peptides were prepared by solid-phase peptide synthesis. Total ion current chromatograms (TIC) and associated mass spectra of purified N-terminal biotinylated SBP1 peptide (A), purified N-terminal biotinylated SBP2 peptide (B), crude SBP1 peptide (C), and crude SBP2 peptide (D).

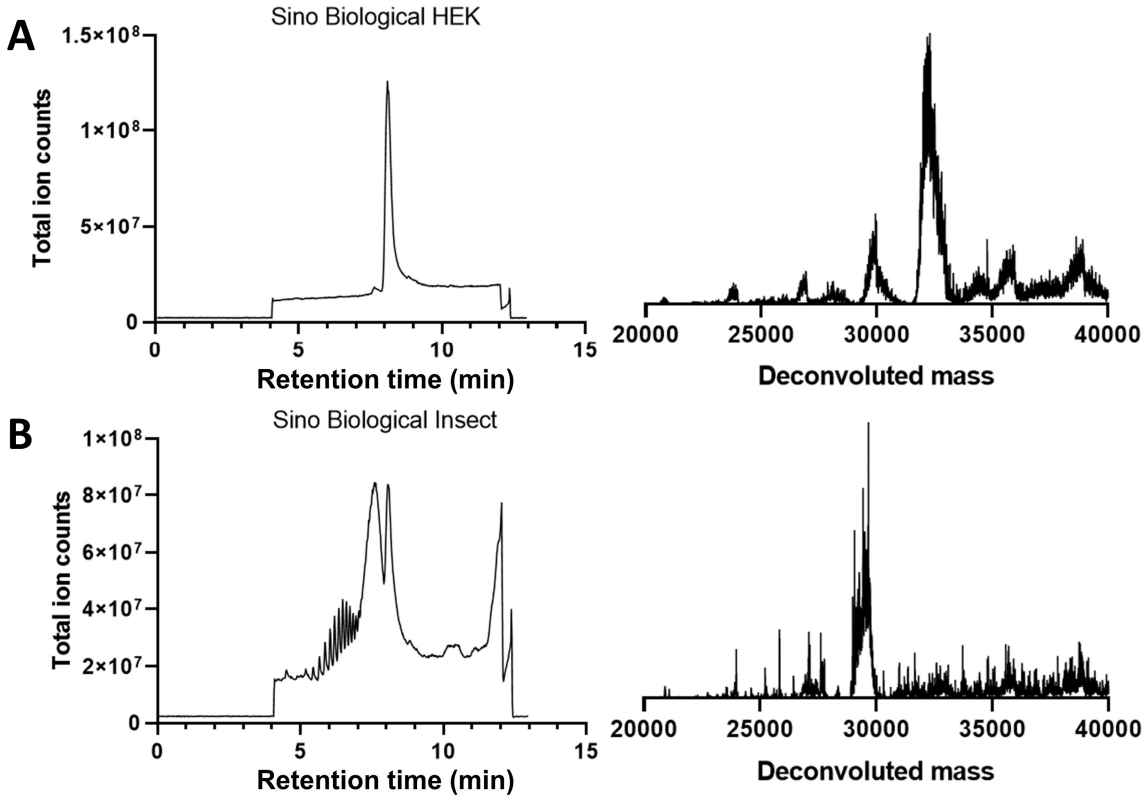

Supplemental Figure 2. SARS-CoV-2 spike protein RBD domains derived from different biological sources display differences in mass distribution profiles. Total ion current chromatograms (TIC) obtained by LC-MS analysis of commercial samples of (A) glycosylated Sino Biological HEK-expressed SARS-CoV-2-RBD (solution in phosphate-buffered saline) and (B) glycosylated Sino Biological insect-derived SARS-CoV-2-RBD with associated deconvoluted mass spectra obtained by integration over the protein peak at ~8 min. The broad bands in the TIC chromatograms of (B) are due to additives present in the vendor-formulated solid powder (10% glycerol, 5% trehalose, 5% mannitol and 0.01% tween-80).

355 ## References

356 1. Li, F., W. Li, M. Farzan, and S.C. Harrison, *Structure of SARS coronavirus spike receptor-binding*
357 *domain complexed with receptor.* Science, 2005. **309**(5742): p. 1864-8.
358 2. Li, W., C. Zhang, J. Sui, J.H. Kuhn, M.J. Moore, S. Luo, S.K. Wong, I.C. Huang, K. Xu, N. Vasilieva, A.
359 Murakami, Y. He, W.A. Marasco, Y. Guan, H. Choe, and M. Farzan, *Receptor and viral*
360 *determinants of SARS-coronavirus adaptation to human ACE2.* EMBO J, 2005. **24**(8): p. 1634-43.
361 3. McCray, P.B., Jr., L. Pewe, C. Wohlford-Lenane, M. Hickey, L. Manzel, L. Shi, J. Netland, H.P. Jia,
362 C. Halabi, C.D. Sigmund, D.K. Meyerholz, P. Kirby, D.C. Look, and S. Perlman, *Lethal infection of*
363 *K18-hACE2 mice infected with severe acute respiratory syndrome coronavirus.* J Virol, 2007.
364 **81**(2): p. 813-21.
365 4. Moore, M.J., T. Dorfman, W. Li, S.K. Wong, Y. Li, J.H. Kuhn, J. Coderre, N. Vasilieva, Z. Han, T.C.
366 Greenough, M. Farzan, and H. Choe, *Retroviruses pseudotyped with the severe acute respiratory*
367 *syndrome coronavirus spike protein efficiently infect cells expressing angiotensin-converting*
368 *enzyme 2.* J Virol, 2004. **78**(19): p. 10628-35.
369 5. Hoffmann, M., H. Kleine-Weber, S. Schroeder, N. Kruger, T. Herrler, S. Erichsen, T.S. Schiergens,
370 G. Herrler, N.H. Wu, A. Nitsche, M.A. Muller, C. Drosten, and S. Pohlmann, *SARS-CoV-2 Cell Entry*
371 *Depends on ACE2 and TMPRSS2 and Is Blocked by a Clinically Proven Protease Inhibitor.* Cell,
372 2020. **181**(2): p. 271-280.
373 6. Walls, A.C., Y.J. Park, M.A. Tortorici, A. Wall, A.T. McGuire, and D. Veesler, *Structure, Function,*
374 *and Antigenicity of the SARS-CoV-2 Spike Glycoprotein.* Cell, 2020. **181**(2): p. 281-292.
375 7. Wrapp, D., N. Wang, K.S. Corbett, J.A. Goldsmith, C.L. Hsieh, O. Abiona, B.S. Graham, and J.S.
376 McLellan, *Cryo-EM structure of the 2019-nCoV spike in the prefusion conformation.* Science,
377 2020. **367**(6483): p. 1260-1263.
378 8. Yan, R., Y. Zhang, Y. Li, L. Xia, Y. Guo, and Q. Zhou, *Structural basis for the recognition of the*
379 *SARS-CoV-2 by full-length human ACE2.* Science, 2020. **367**(6485): p. 1444-1448.
380 9. Smith, M.C. and J.E. Gestwicki, *Features of protein-protein interactions that translate into potent*
381 *inhibitors: topology, surface area and affinity.* Expert Rev Mol Med, 2012. **14**: p. e16.
382 10. Josephson, K., A. Ricardo, and J.W. Szostak, *mRNA display: from basic principles to macrocycle*
383 *drug discovery.* Drug Discov Today, 2014. **19**(4): p. 388-99.
384 11. D.P. Han, A. Penn-Nicholson, and M.W. Cho, *Identification of critical determinants on ACE2 for*
385 *SARS-CoV entry and development of a potent entry inhibitor*. Virology, 2006. **350**: p. 15-25.
386 12. S. Xia, L. Yan, W. Xu, A.S. Agrawal, A. Algaissi, C.K. Tseng, Q. Wang, L. Du, W. Tan, I.A. Wilson, S.
387 Jiang, B. Yang, and L. Lu, *A pan-coronavirus fusion inhibitor targeting the HR1 domain of human*
388 *coronavirus spike*. Science Advances, 2019. **5**: p. eaav4580.
389 13. Xia, S., Liu, M., Wang, C. et al., *Inhibition of SARS-CoV-2 (previously 2019-nCoV) infection by a*
390 *highly potent pan-coronavirus fusion inhibitor targeting its spike protein that harbors a high*
391 *capacity to mediate membrane fusion*. Cell Res, 2020. **30**: p. 343-355.
392 14. M. Romano, A. Ruggiero, F. Squeglia, and R. Berisio, An engineered stable mini-protein to plug
393 SARS-Cov-2 Spikes. BioRxiv, 2020. Preprint: https://doi.org/10.1101/2020.04.29.067728.
394 15. Hartrampf, N., Saebi, A., Poskus, M., Gates, Z.P., Callahan, A.J., Cowfer, A.E., Hanna, S., Antilla,
395 S., Schissel, C.K., Quartararo, A.J., Ye, X., Mijalis, A.J., Simon, M.D., Loas, A., Liu, S., Jessen, C.,
396 Nielsen, T.E., Pentelute, B.L. , *Synthesis of proteins by automated flow chemistry.* Science, 2020.
397 **368**(6494): p. 980-987.
398 16. *Amber 2019 reference manual.* https://ambermd.org/doc12/Amber19.pdf.

399 17. Mijalis, A.J., D.A. Thomas, 3rd, M.D. Simon, A. Adamo, R. Beaumont, K.F. Jensen, and B.L.
400 Pentelute, *A fully automated flow-based approach for accelerated peptide synthesis.* Nat Chem
401 Biol, 2017. **13**(5): p. 464-466.
402 18. Wojcik, P. and L. Berlicki, *Peptide-based inhibitors of protein-protein interactions.* Bioorg Med
403 Chem Lett, 2016. **26**(3): p. 707-713.
404 19. Jenny-Avital, E.R., *Enfuvirtide, an HIV-1 fusion inhibitor.* N Engl J Med, 2003. **349**(18): p. 1770-1.
405 20. Wan, Y., J. Shang, R. Graham, R.S. Baric, and F. Li, *Receptor recognition by novel coronavirus*
406 *from Wuhan: An analysis based on decade-long structural studies of SARS.* J Virol, 2020. DOI:
407 10.1128/JVI.00127-20.
408 21. Y. Watanabe, J.D. Allen, D. Wrapp, J.S. McLellan, and M. Crispin, *Site-specific glycan analysis of*
409 *the SARS-CoV-2 spike*. Science, 2020. p. eabb9983.
410 22. Touti, F., Z.P. Gates, A. Bandyopadhyay, G. Lautrette, and B.L. Pentelute, *In-solution enrichment*
411 *identifies peptide inhibitors of protein-protein interactions.* Nat Chem Biol, 2019. **15**(4): p. 410-
412 418.